ROYAL SOCIETY
OF CHEMISTRY

PAPER

Check for updates

Enhancing mechanical-to-charge conversion in triboelectric nanogenerators

Linglin Zhou,†[ab] Di Liu,†[c] Yikui Gao,[ab] Wenyan Qiao,[ab] Dongyang Liu,[a] Zhihao Zhao, [ID][ab] Lijiang Yin,[ab] Xinyuan Li,[ab] Zhong Lin Wang[abde] and Jie Wang [ID]*[abd]

Triboelectric nanogenerators (TENGs) hold transformative promise for renewable energy harvesting and as power sources for the Internet of Things. However, a key challenge remains in concurrently enhancing their output energy and energy conversion efficiency, especially at high triboelectric charge densities. Here, our study reveals that increased frictional heat and electrostatic force at elevated charge densities lead to greater energy dissipations, thereby limiting efficiency improvements. To address this issue, we introduce a novel metric, the mechanical-to-charge conversion factor (f_{M-Q}), which quantitatively correlates surface charge density with friction force. This enables simultaneous assessment and optimization of output energy and energy conversion efficiency. Assisted by strategic material selection and interfacial lubrication, this synergy elevates f_{M-Q} by 7.8-fold, achieving a remarkable 17-fold enhancement in energy conversion efficiency and a record-breaking energy density of 11.9 J m^{-2} cycle^{-1}. This work provides new insights into advancing practical triboelectric technologies with benefits of both performance and efficiency.

Broader context

Mechanical energy conversion and utilization have been pivotal throughout human technological evolution, from ancient friction-based fire-starting to modern triboelectric nanogenerators (TENGs) in the Internet of Things era. However, the relationship between triboelectric charge density and energy conversion efficiency remains unclear. This study shows that higher charge density in TENGs often reduces efficiency due to increased frictional heat and electrostatic forces, causing greater energy dissipation. To solve this, we propose a fundamental mechanism linking driving force and charge density, enabling simultaneous optimization of output energy and conversion efficiency. This is quantified by the mechanical-to-charge conversion factor (f_{M-Q}), which serves as a key performance metric. The f_{M-Q} factor provides quantitative criteria for evaluating TENGs, enhancing our understanding of mechanoelectrical conversion. Our approach allows co-optimization of electrical output and energy utilization, improving TENG performance for self-powered systems and portable electronics. By balancing charge density and driving force, we mitigate efficiency losses while maximizing power generation. This work not only clarifies the physics behind TENG limitations but also offers a practical strategy for designing more efficient energy harvesters. The f_{M-Q} framework opens new pathways for developing high-performance mobile power source, advancing applications in IoT and wearable technologies.

Introduction

Mechanical energy conversion and utilization have played critical roles through human technological revolution, from ancient practices like using friction to ignite fire based on mechanical energy conversion into thermal energy, to modern innovations such as triboelectric nanogenerators (TENGs) that harness triboelectrification and electrostatic induction for power generation in the new era of the Internet of Things.[1] The key distinction lies in the objectives: ancient methods aim to maximize thermal energy acquisition, whereas contemporary TENGs focus on maximizing electrical energy utilization. Over millennia, methods to improve the success rate and efficiency of drill wood to fire, such as using dry wood and increasing friction force and friction velocity have been well-documented. However, simultaneously enhancing the output performance and efficiency of TENGs remains a significant challenge.

TENGs harness the triboelectric effect, coupled with electrostatic induction, to directly convert ubiquitous mechanical

[a] *Beijing Institute of Nanoenergy and Nanosystems, Chinese Academy of Sciences, Beijing 101400, P. R. China. E-mail: wangjie@binn.cas.cn*

[b] *College of Nanoscience and Technology, University of Chinese Academy of Sciences, Beijing 100049, P. R. China*

[c] *Department of Mechanical Engineering, The Hong Kong Polytechnic University, Hong Kong 999077, P. R. China*

[d] *Guangzhou Institute of Blue Energy, Knowledge City, Huangpu District, Guangzhou 510555, P. R. China*

[e] *Yonsei Frontier Lab, Yonsei University, Seoul 03722, Republic of Korea*

† Linglin Zhou and Di Liu contributed equally.

This journal is © The Royal Society of Chemistry 2025

Energy Environ. Sci., 2025, **18**, 10403–10412 | **10403**

energy into electrical energy,[2–6] opening up a new avenue for renewable energy harvesting. In the process of triboelectricity, tribo-material pairs acquire equal and opposite charges due to differences in their surface electron affinities. Given the quadratic correlation between output power density and surface charge density,[7] significant efforts have been directed towards enhancing the surface charge density of TENGs to boost their output power. Strategies including material optimization,[8–10] structural design,[11–17] environmental control,[18–20] and charge excitation methods[21–23] have led to unprecedentedly high surface charge densities, reaching several mC m^{-2}. However, these surface charges also elevate frictional forces by inducing electrostatic attraction between tribo-material pairs, a phenomenon widely observed at metal/polymer,[24] ceramic/polymer,[25] and polymer/polymer[26] interfaces. On one hand, the increased friction between tribo-material pairs boosts triboelectric charge density, which undoubtedly enhances output performance, on the other hand, the elevated triboelectric charge density enhances electrostatic attraction force, friction heat, and material wear,[27–29] leading to enhanced energy dissipations. Consequently, although a high energy conversion (>50%) has been achieved at a low charge density (<30 μC m^{-2}),[30] whether higher energy conversion efficiency can be achieved at high triboelectric charge density remains an opening question, necessitating further investigation into this fundamental issue to ultimately enable substantial improvements in the performance and efficiency of TENGs.

Here, we demonstrate that energy dissipation in TENGs escalates at elevated charge densities, primarily driven by severely frictional heating and stronger electrostatic forces, leading to the inherent trade-off between output energy and energy conversion efficiency in TENGs. To address this limitation, we propose a quantitative metric as mechanical-to-charge conversion factor (f_{M-Q}), providing systematic guidance for co-optimizing electrical output and energy utilization. Guided by this metric, the strategic integration of dielectric material selection with interfacial lubrication design demonstrates remarkable efficacy in suppressing energy dissipation while enhancing charge tapping capability, thereby elevating f_{M-Q} by 7.8 times (from 51 to 396). Consequently, we achieved a remarkable 17-fold increase in energy conversion efficiency of TENGs, with a record-breaking energy density of 11.9 J m^{-2} cycle^{-1} at a high surface charge density of 1 mC m^{-2}. These findings deepen our understanding of the relationship between electrical output characteristics and mechanoelectrical conversion in TENGs. Furthermore, this work provides a new perspective for reducing friction-related energy loss in TENGs, thereby enhancing energy conversion efficiency and output performance.

Results and discussion

The concept of mechanical-to-charge conversion in TENGs

Triboelectric nanogenerators (TENGs) efficiently convert mechanical energy into electrical energy through the coupling effects of triboelectrification and electrostatic induction.

However, the process of triboelectrification inevitably raises the surface temperature of triboelectric materials, similar to the principle underlying friction fire-making (Fig. 1a), leading to energy loss in the form of heat. Additionally, the process of electrostatic induction can be accompanied by electrostatic breakdown,[31–33] particularly at high surface charge densities, causing further energy loss in the form of electrostatic breakdown (Fig. 1b). Theoretical analysis of the effect of surface temperature on interfacial friction indicates that rising surface temperatures enlarge the actual contact area between tribo-pairs, resulting in a higher charge density and subsequently intensified friction (Fig. 1c, and Fig. S1, S2 and Note S1). Consequently, the relationship between surface charge density and thermal energy loss due to friction in TENGs can be summarized as follows (Fig. 1d). On one hand, increased mechanical input enhances surface charge density, thereby augmenting interfacial friction through increased electrostatic attraction. This process results in a rise in surface temperature due to friction-induced heating. The temperature increase serves as a dual purpose: it facilitates charge transfer, thereby boosting surface charge density, and it enlarges the actual contact area between tribo-material pairs, further intensifying interfacial friction and promoting triboelectric charging. On the other hand, while greater mechanical input increases surface charge density, it also heightens thermal energy generation through friction-induced heating. Furthermore, at elevated surface charge densities, the increased actual contact area, driven by both frictional heating and enhanced electrostatic forces, significantly contributes to thermal energy consumption. Therefore, minimizing these friction-induced energy consumptions is crucial for improving electric output performance and enhancing energy conversion efficiency. However, the primary challenge is the lack of an effective method for simultaneously assessing the electric output performance and energy conversion efficiency of TENGs.

Based on the relationship between mechanical energy input and electrical energy output, the energy conversion efficiency of TENG (η) can be described as (Note S2):

$$\eta = \frac{E_{out}}{E_{in}} = k\frac{\sigma^2}{F_f} \times 100\% \tag{1}$$

where k is a constant that represents the structural and material parameters of designed TENGs, σ is the surface charge density, F_f is the interfacial friction force. According to eqn (1), we plot the surface charge density–friction force (σ–F_f) curves for various material pairs (Fig. 1e and Fig. S3), and find some interesting patterns. For triboelectric pairs with weak triboelectric properties, such as ethyl tetra fluoro ethylene (ETFE)-ETFE and polyamides (PA)-PA, increasing the applied force primarily enhances the friction force without affecting the surface charge density. This behavior is analogous to the principle of ancient fire-by-friction techniques, with the corresponding σ–F_f curves falling within the blue region. In contrast, for triboelectric pairs with strong triboelectric properties, like PA–ETFE, a larger applied force leads to an increase in both friction force and surface charge density, positioning the σ–F_f

10404 | *Energy Environ. Sci.*, 2025, **18**, 10403–10412

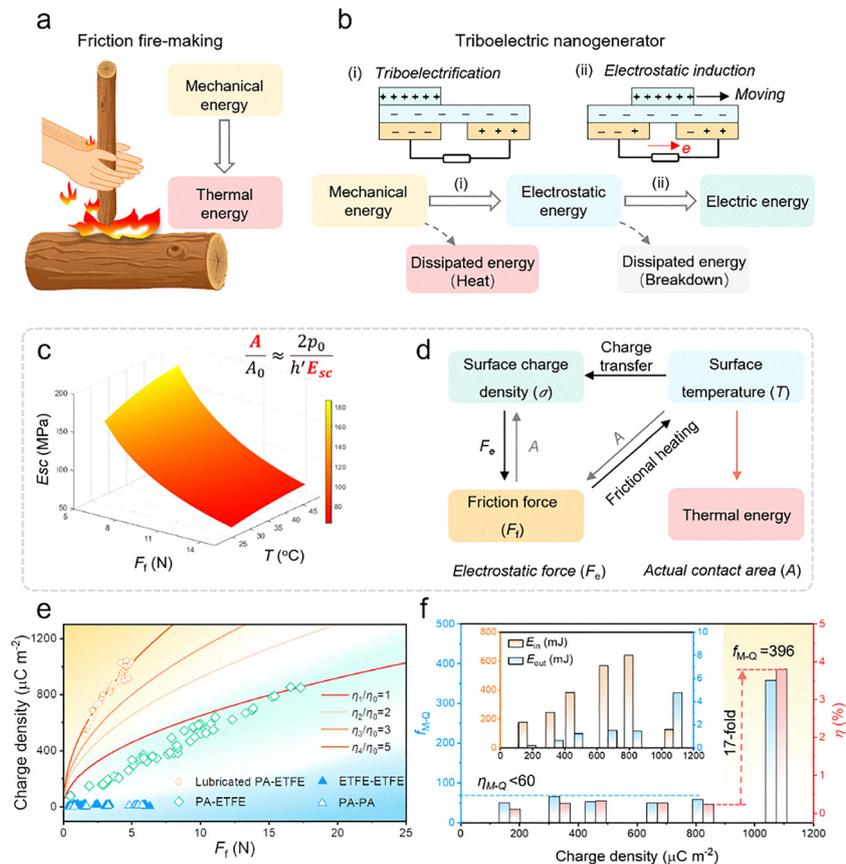This journal is © The Royal Society of Chemistry 2025

Fig. 1 The concept of mechanical-to-charge conversion in TENGs. (a) Energy flow chart of friction fire-making process, where mechanical energy is converted to thermal energy. (b) Energy flow chart of TENG system at high surface charge density value, where mechanical energy is converted to electric energy. In this process, friction induces energy dissipation in the way of heat and electrostatic breakdown. (c) A schematic of the mechanism underlying the surface temperature effect on the frictional force, revealing that an increase in surface temperature expands the actual contact area between tribo-pairs, subsequently intensifying friction. (d) Schematic diagram shows the relationship among the surface charge density, friction force and the production of thermal energy by influencing electrostatic force and actual contact area between the tribo-materials. (e) σ–F_f curve showing the optimized direction of mechanical-to-charge conversion in TENG. (f) A higher $f_{M–Q}$ of TENG enables both high output energy and energy conversion efficiency. The inset illustrates the variation of both energy input and energy output as the surface charge density increases.

curve in the green region. This shift contributes to an increase in both thermal energy loss due to higher surface temperatures and increased electric energy output. By utilizing an interfacial lubrication strategy, we aim to further increase the surface charge density while simultaneously reducing the friction force, shifting the PA–ETFE curve upwards and towards the upper left yellow region. These findings suggest that the σ–F_f curve is a crucial indicator for optimizing the output performance and mechanical input of TENGs. Therefore, we define the ratio of σ and F_f as mechanical-to-charge conversion factor ($f_{M–Q}$).

Additionally, $f_{M–Q}$ can serve as an accurate indicator of the energy conversion efficiency of TENGs, as demonstrated in σ–F_f curves. To streamline the evaluation of energy conversion efficiency, we propose a normalized metric-relative energy conversion efficiency (η_n/η_0) that temporarily circumvents complexities related to structural design and material selection, thereby providing a focused framework for optimization (Fig. 1e and Note S3). A value of η_n/η_0 greater than 1 signifies an improvement in TENGs' energy conversion efficiency. Notably, as η_n/η_0

increases, its corresponding curve shifts toward the upper-left yellow region, which represents higher $f_{M–Q}$ values. This trend demonstrates that an elevated $f_{M–Q}$ correlates with enhanced energy conversion efficiency. Based on above analyses, for a designed TENG, a higher $f_{M–Q}$ not only reflects superior output performance but also indicates improved energy conversion efficiency, making it a comprehensive metric for evaluating TENGs' performance across multiple dimensions. However, it is important to note that merely increasing the surface charge density does not elevate the energy conversion efficiency, as η_n/η_0 remains below 1 (Fig. 1e, f and Fig. S4, S5 and Note S4). Notably, even at an applied force of 20 N, the ratio η_1/η_0 remains limited at 1 due to the concurrent rise in charge density and friction force (Fig. S6). Guid by this metric, we employ tribo-materials optimization and interfacial lubrication to reduce friction-induced energy losses and enhance output energy, which increases $f_{M–Q}$ by 7.8 times and leads to a 17-fold enhancement in energy conversion efficiency with a record-breaking energy density of 11.9 J m^{-2} cycle^{-1}.

This journal is © The Royal Society of Chemistry 2025

Energy Environ. Sci., 2025, **18**, 10403–10412 | **10405**

Tribo-charges amplify friction in TENGs

Although triboelectrification-induced interfacial wear has been extensively documented in conventional systems operating at low charge densities, the energy dissipation pathways under high charge density conditions, such as for TENGs, remain poorly understood. We select the working mode of FS-TENG, that mainly consists of PA–ETFE tribo-material pairs and a back electrode, to examine the correlation between transferred charges and frictional force (F_f) due to its superior output performance. Besides, electrode's edge-adhered insulator layer design is implemented to improve the surface charge density by elevating the Coulombic efficiency.[11] The working mechanism of FS-TENG is illustrated in Fig. S7 and Note S5. Previous research has reported that the electrostatic attraction force induced by tribo-charges between tribo-materials is one of the factors affecting friction, which is confirmed in the non-contact mode TENG (Fig. 2a and b). A similar phenomenon is also

discovered in the contact mode TENG with low output by using identical tribo-materials of ETFE (inset of Fig. 2c). As the surface charge varying from 5 nC to 50 nC, the friction force is also improved from 0.54 N to 1.5 N (Fig. 2c and d). At elevated charge outputs, the influence of tribo-charges on friction becomes increasingly significant. Utilizing PA and ETFE as tribo-materials under a load of 10 N yields a high output of 350 nC (inset of Fig. 2e). During repeated friction cycles, the frictional force increases as the transferred charge accumulates from the 1st to 16th cycle (Fig. 2e and Fig. S8). However, when surface charge is discharged to approximate its initial value (Fig. S9), the friction force experiences a sharp decline (Fig. 2e and Fig. S8). It is noteworthy that the increased friction force after discharging, relative to its initial value, may be attributed to the increase in actual contact area under high surface charge density, which is resulted from irreversible plastic deformation of the dielectric thin-film material (Fig. 2f). Notably, electrostatic forces play a crucial role in charge-induced amplification
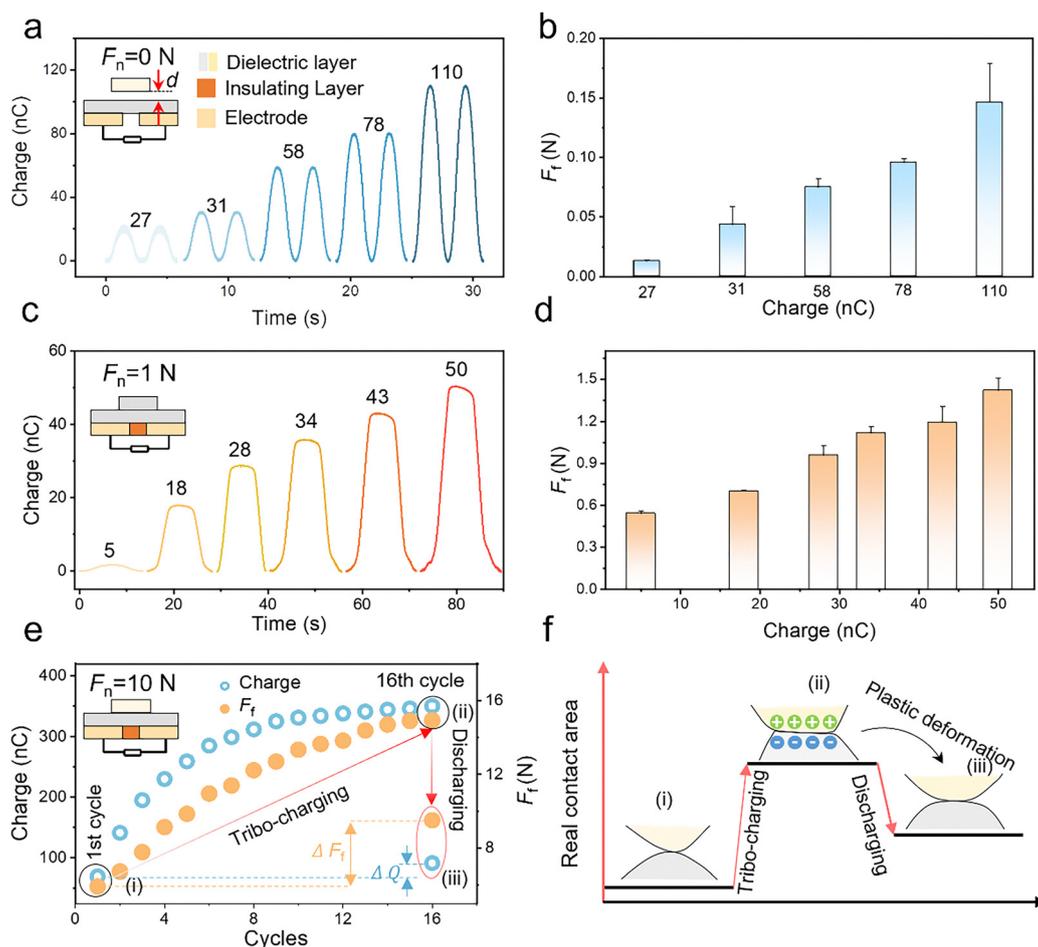

Fig. 2 Tribo-charges amplify friction in TENGs. (a) and (b) The transferred charges (a) and corresponding F_f (b) at different transferred charges of non-contact mode FS-TENG without external normal force. (c) and (d). The transferred charges (c) and corresponding F_f (d) at different transferred charges of contact mode FS-TENG at normal force of 1 N. (e) The schematic diagram, transferred charges, and corresponding F_f at different operation cycles of TENG at normal force of 10 N. F_f increases as the transferred charge accumulates from the 1st to 16th cycle. However, when eliminates the surface charges of TENG to approximating its initial value, the final F_f experiences a sharp decline. (f) The change of actual contact area during the tribo-charging and discharging process in TENG, where electrostatic friction under high surface charge density increases the actual contact area because of an irreversible plastic deformation of the dielectric thin-film material.

10406 | *Energy Environ. Sci.*, 2025, **18**, 10403–10412

This journal is © The Royal Society of Chemistry 2025

of friction, though their quantitative mechanistic role remains systematically uncharacterized.

Friction-related energy dissipation in TENGs

We subsequently examined how the enhancement of frictional force, induced by charge density, affects energy dissipation in TENGs. By employing the ion injection method, we successfully achieved three distinct transferred charges of 60 nC, 120 nC, and 200 nC (Fig. S10), corresponding to F_f of 0.07 N, 0.27 N, and 0.49 N, respectively (Fig. S12a). Despite a minor decline of 200 nC after 5000 cycles due to insufficient triboelectric replenishment, the high-charge output (170 nC) remained significantly higher than the other two charge outputs. Thus, the consistent retention capability across these three distinct charge densities provides a solid foundation for subsequent in-depth exploration of the impact of different charge outputs on friction-induced energy loss (Fig. S11b). After 5000 cycles of operation, the increased roughness and severe scratching observed on both ETFE and PA surfaces at higher transferred charges suggest that high surface charge density in TENGs leads to a greater conversion of mechanical energy into the internal energy of material *via* friction and wear, thereby contributing to energy loss (Fig. 3a and Fig. S11c). More importantly, the surface temperature of PA increases with transferred charges (Fig. 3b). Before the triboelectric process, the temperature of the PA surface remains at room temperature ($\sim$23 °C).

After 50 operational cycles, the surface temperature of PA increased to 28.3 °C, 28.9 °C, and 31.0 °C, corresponding to transferred charges of 60 nC, 120 nC, and 200 nC, respectively. This suggests that the conversion of mechanical energy to thermal energy is another major source of energy loss in TENG, consistent with previous analysis. In all, the observed intensification of energy dissipation under elevated surface charge densities originates fundamentally from the expansion of real contact area, which could relate to two energy-loss pathways (Fig. 3c and d): (i) material internal energy accumulation *via* wear-induced plastic deformation and (ii) thermal energy generation through frictional heating and interfacial heat transfer.

Minimizing energy dissipation for TENG

Guided by the theoretical analysis of $f_{M–Q}$ values, achieving simultaneous enhancement of electric output and energy conversion efficiency in TENGs requires stabilizing charge density, suppressing wear, and reducing heat generation, ultimately
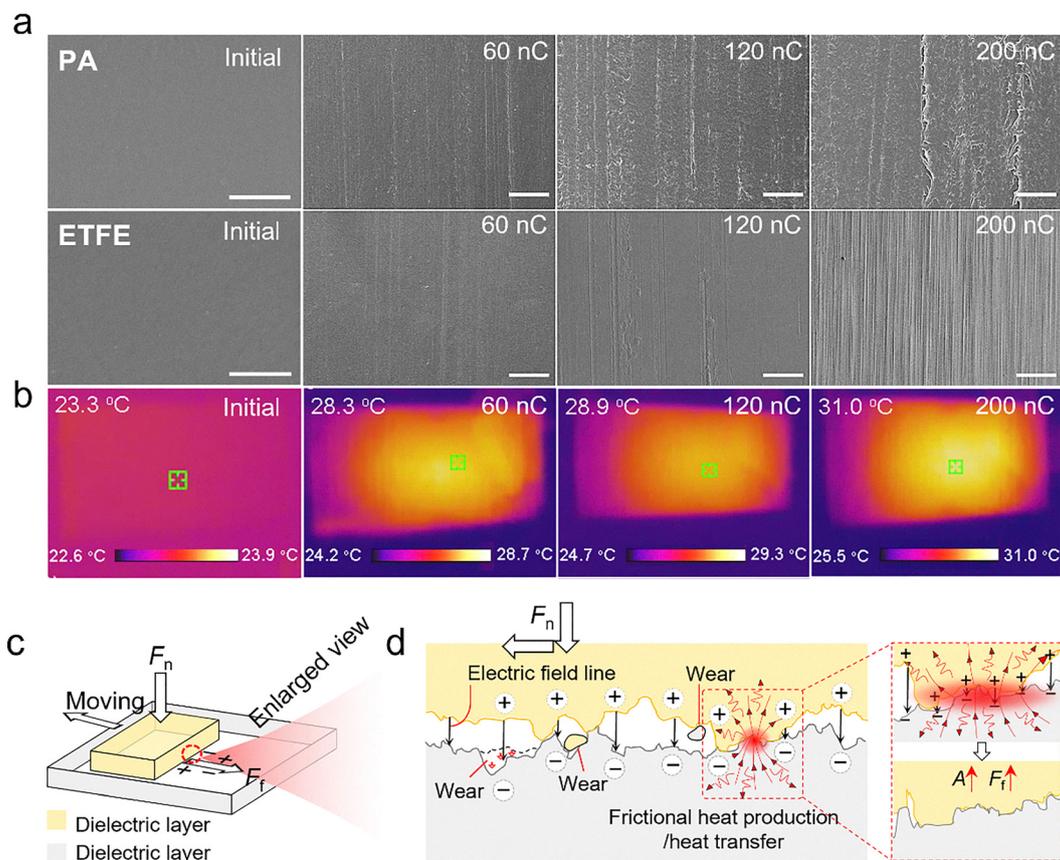

Fig. 3 Friction-related energy dissipation in TENGs. (a) SEM images of PA and ETFE after 5000 cycles under different charges, indicating that elevated triboelectric charge density enhances materials wear. The scale bar for TEM images is 20 μm. (b) Thermal camera images of the PA surface under different transferred charges, indicating that elevated triboelectric charge density enhances friction heat, leading to enhanced energy dissipations. (c) and (d) Schematic diagram show energy dissipation (including wear and heat production/transfer) induced by enlarged real contact area at high charge density.
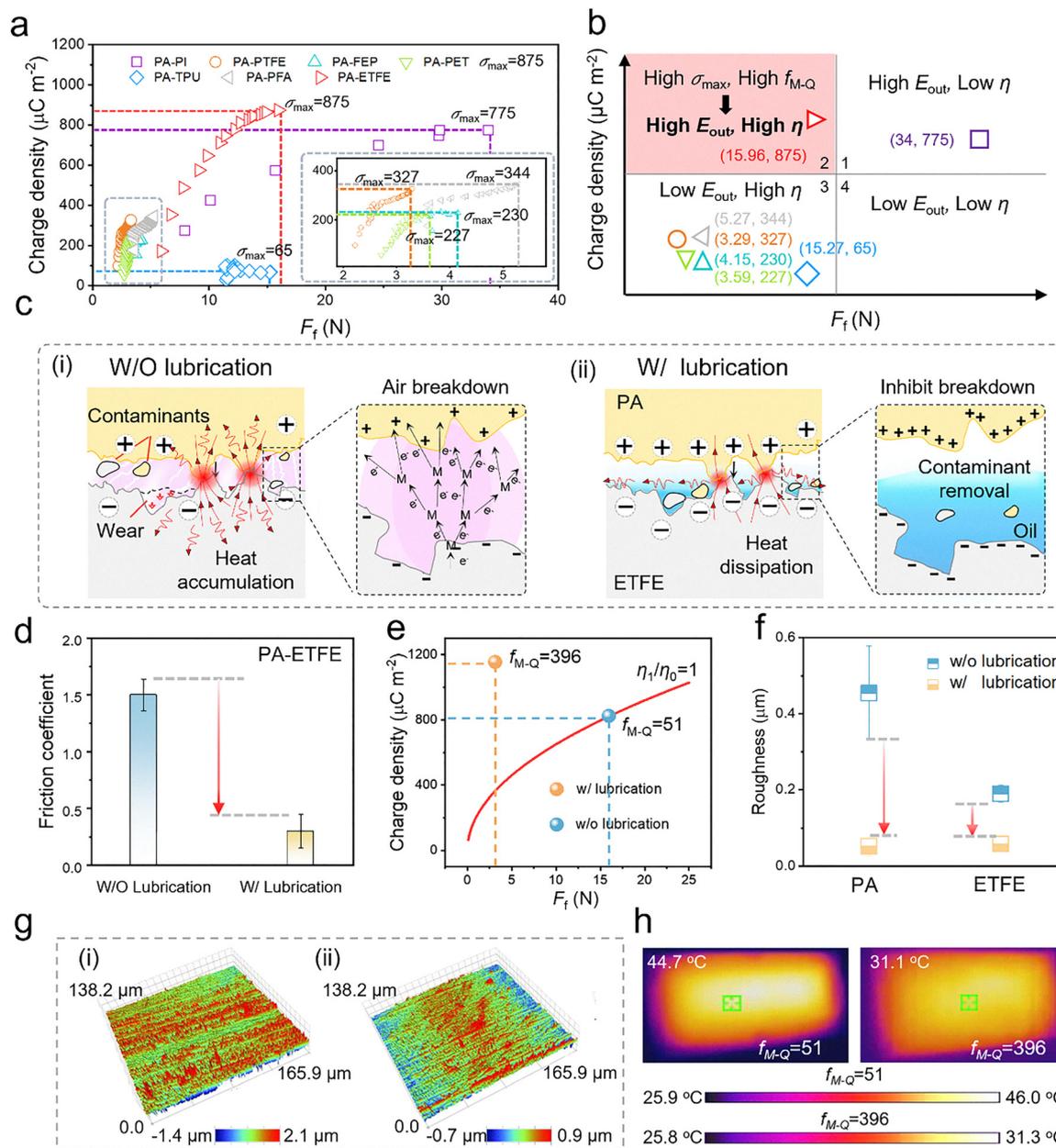
This journal is © The Royal Society of Chemistry 2025

Energy Environ. Sci., 2025, **18**, 10403–10412 | **10407**

Fig. 4 Improvement of the mechanical-to-charge conversion by minimizing energy dissipation. (a) $\sigma-F_f$ curves of different tribo-pairs. Tribo-pairs in the upper-left quadrant (*e.g.*, PA–ETFE) achieve both a high σ_{max} and a high f_{M-Q}, enabling superior performance in both energy output and energy conversion efficiency compared to other tribo-pairs. (b) Four quadrants of the $\sigma-F_f$ diagram. Material pairs located in the second quadrant meet the criteria for both high σ_{max} and f_{M-Q}, thereby enabling the achievement of both high output performance and superior energy conversion efficiency for TENG. (c)–(g) Achieving high f_{M-Q} by minimizing energy dissipation *via* interface lubrication: (c) schematic diagram shows eliminating energy dissipation including air breakdown, heat accumulation and wear by liquid lubrication, (d) the comparison of μ between TENG with and without interface lubrication, (e) the effect of interface lubrication on f_{M-Q} of PA–ETFE, *f* roughness of PA and ETFE at different f_{M-Q}, (g) 3D optical surface profiler images of PA ((i): f_{M-Q} = 51, (ii) f_{M-Q} = 396), h the frictional heat on PA at different f_{M-Q}.

addressing the historical trade-off between charge density and energy conversion efficiency. To validate this, we combined seven representative negative polarity materials (ETFE, PTFE, polyimide (PI), fluorinated ethylene propylene (FEP), polyfluoroalkoxy (PFA), polyethylene terephthalate (PET), thermoplastic urethanes (TPU)) with the positive polarity materials of PA to fabricate FS-TENG. As depicted in Fig. 4a, b and Table S1, if

tribo-pairs positioned in the lower-right quadrant exhibit the high friction force and low triboelectric performance, resulting in both lower f_{M-Q} and maximum surface charge density (σ_{max}), and thus both low output energy and energy conversion efficiency (Fig. S12). In contrast, tribo-pairs positioned in the lower-left quadrant (*e.g.*, PA–PTFE, PA–FEP, PA–PET, PA–TPU, and PA–PFA) display a high f_{M-Q} but a low σ_{max}, leading to

TENGs with high energy conversion efficiency yet relatively low energy output (Fig. S12). On the other hand, tribo-pairs in the upper-right quadrant (*e.g.*, PA–PI) achieve a high σ_{max} but a low $f_{M–Q}$, resulting in TENGs with higher energy output but diminished energy conversion efficiency (Fig. S12). Notably, tribo-pairs in the upper-left quadrant (*e.g.*, PA–ETFE) achieve both a high σ_{max} and a high $f_{M–Q}$, enabling superior performance in both energy output and energy conversion efficiency compared to other tribo-pairs. The corresponding friction force, charge accumulation process, and output energy cycles of various tribo-pairs are shown in Fig. S13. Based on these findings, if the σ–F_f diagram is divided into four quadrants, tribo-material pairs located in the second quadrant should be prioritized during material selection, as they simultaneously meet the criteria for both high σ_{max} and high $f_{M–Q}$, thereby enabling the achievement of both high output performance and superior energy conversion efficiency for TENGs (Fig. 4b). Following the selection of these tribo-pairs, the next critical question arises: how can further optimization strategies be implemented to enhance the energy conversion efficiency while maintain the high surface charge density?

Taking the electrostatic force induced by surface charges into account,[34] the energy conversion efficiency of TENGs can be formulated as follows (Note S6):

$$\eta = k \frac{\sigma^2}{\mu(F_e + F_n)x} \times 100\% \tag{2}$$

where μ denotes the friction coefficient, F_e represents the electrostatic force component acting in the vertical direction, F_n represents the normal force, and x is the displacement. Among various parameters, σ serves as the primary indicator of TENG's output performance. Notably, F_n, x, and F_e remain almost constant when σ is fixed. Therefore, achieving a high energy conversion efficiency can be facilitated by reducing the friction coefficient (Fig. S14).

The most effective strategy for reducing friction coefficient at the friction interface of TENGs is interface lubrication (Fig. S15). Compared to TENGs without liquid lubrication, the application of lubricating oil with a lower friction coefficient at the TENG interface can minimize friction-related energy losses through two key strategies: (i) reducing tribo-charging-induced material wear by contaminant removal, (ii) declining heat generation and accumulation for effectively dissipation into the environment *via* the cooling system (Fig. 4c). Our previous work has been reported that compared to air dielectric layers, lubricating oil, characterized by its higher breakdown field strength, can effectively suppress the electrostatic breakdown phenomenon,[35] thereby enhancing the output energy of TENGs. Consequently, these dual effects of interface lubrication improve mechanical-to-charge conversion of TENGs.

As illustrated in Fig. 4d and Fig. S16, TENGs with lower friction coefficient exhibits a 30% increase in charge density and a 3.4-fold reduction in friction force compared to the initial device. Consequently, it achieves an increasement of $f_{M–Q}$ from 51 to 396 (Fig. 4e), indicating that interface lubrication enhances both the output energy and energy conversion of

TENGs. The underlying mechanism is demonstrated through changes in wear properties and heat production at the tribo-pair interface. After 6000 stability tests with lubrication, the surface roughness of PA and ETFE decreases from 0.46 μm to 0.05 μm and from 0.19 μm to 0.06 μm, respectively (Fig. 4f). Additionally, the wear height difference of PA and ETFE decline from 2.1 μm to 0.9 μm and from 1.1 μm to 0.9 μm, respectively, when liquid lubrication is applied (Fig. 4g(i)–(ii) and Fig. S17). Regarding heat generation during operation of TENGs, the temperature on the lubricated PA surface (31.1 °C) shows a significant decrease compared to the unlubricated device (44.7 °C) (Fig. 4h).

Achieving high mechanical-to-charge conversion for TENG

Following the enhancement of $f_{M–Q}$ by minimizing energy dissipation, we investigated the subsequent changes in output energy and energy conversion efficiency. After interface lubrication, $f_{M–Q}$ increased from 51 to 396, while the input mechanical energy of TENGs decreased by a factor of 5.1, from 638.83 mJ to 124.73 mJ, compared to the unlubricated device (Fig. 5a). The maximum output energy of TENG was achieved at a resistance of 10 GΩ (Fig. 5b and c). Beyond this resistance, breakdown peaks were observed, suggesting that further increases in resistance could compromise the accuracy of output energy measurements (Fig. S18). Notably, the maximum output energy of TENG with a higher $f_{M–Q}$ increased by a factor of 2.4, from 1.40 μJ to 4.76 μJ, when liquid lubrication was applied (Fig. 5b and c). This improvement can be attributed to the inhibition of significant breakdown at both the interface and electrode edge at large resistances due to interface lubrication (11, 31). This is further evidenced by the reduced charge transfer in non-lubricated TENGs compared to the nearly stable charge transfer in lubricated TENGs (Fig. S19). Additionally, the enhanced Coulombic efficiency of lubricated TENGs within the resistance range of 1 GΩ to 10 GΩ, compared to the non-lubricated TENGs (Fig. 5d and Table S2), provides further validation for these findings.

Moreover, the energy conversion efficiency of lubricated TENGs is significantly enhanced across a range of resistance values (Fig. 5e). This improvement is more pronounced at higher resistances, where the breakdown phenomena is effectively suppressed. Specifically, at a resistance of 10 GΩ, the energy conversion efficiency of lubricated TENGs increases by 17-fold, rising from 0.21% to 3.8%, compared to unlubricated devices. Notably, this observed increase (17-fold) significantly exceeds the theoretical prediction of 12-fold (Note S7). This discrepancy may be attributed to the convective effect of the lubricating oil at the interface, which promotes heat transfer from high-temperature to low-temperature regions and dissipates heat into the environment through the cooling system. Additionally, the reduction in wear at higher $f_{M–Q}$ significantly improves the stability of TENGs compared to low $f_{M–Q}$ value (Fig. 5f). Consequently, although the potential issues associated with applying oil lubrication (Note S8), the reduction in frictional heat generation and wear further contributes to the enhanced energy conversion efficiency. By optimizing the
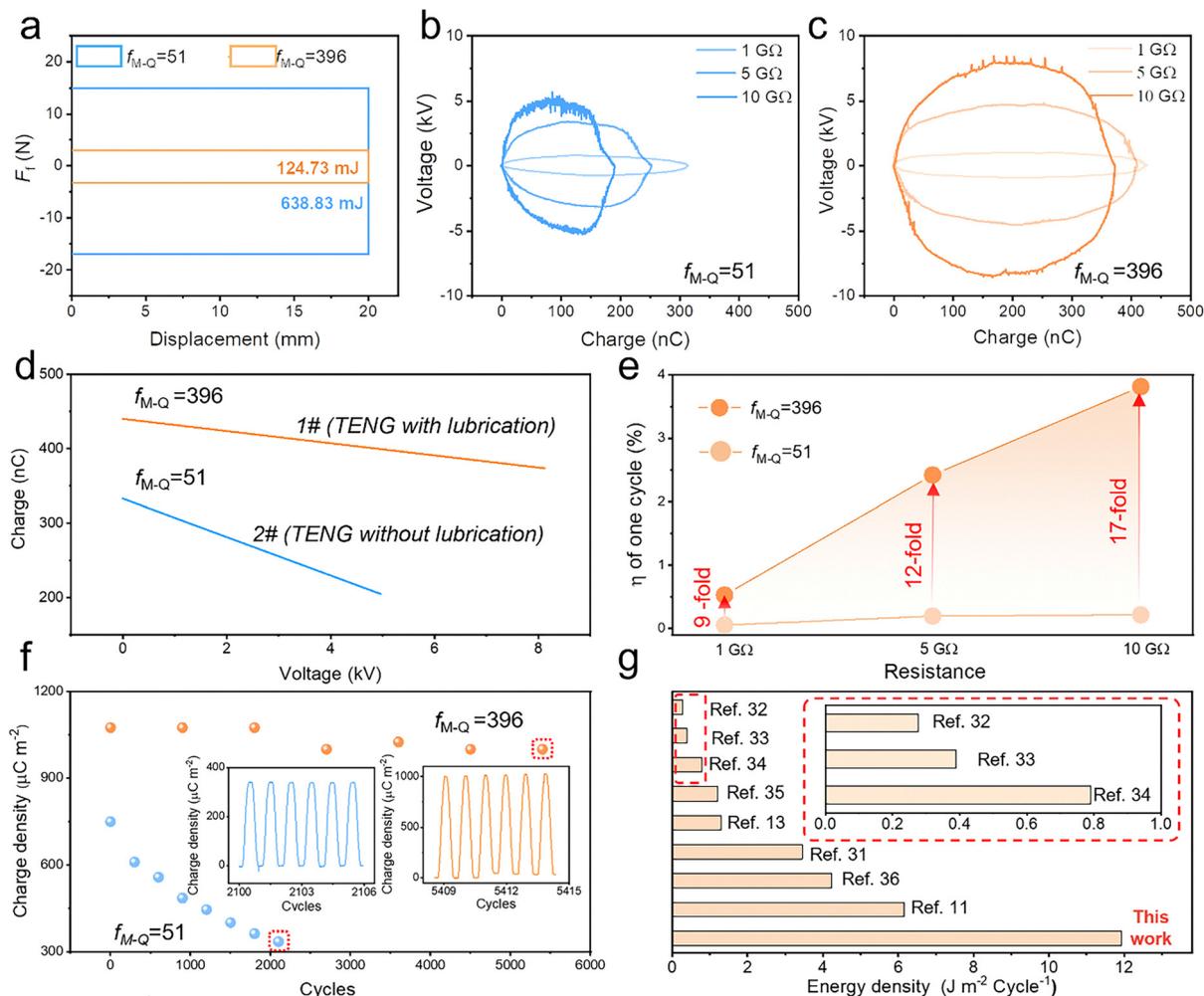
This journal is © The Royal Society of Chemistry 2025

Energy Environ. Sci., 2025, **18**, 10403–10412 | **10409**

Fig. 5 Achieving high energy and improved energy conversion for TENG. (a) The input mechanical energy of TENG with ($f_{M-Q} = 396$) and without ($f_{M-Q} = 51$) interface lubrication under 10 N, where a lower input mechanical energy is achieved at high η_{M-Q}. (b) and (c) The output energy of TENG without ($f_{M-Q} = 51$) b and with ($f_{M-Q} = 396$) (c) interface lubrication under various resistances ranging of 1 GΩ to 10 GΩ. All output energy of lubricated TENGs is higher than that of TENG without lubrication. (d) $Q-V$ curves of TENGs with different parameters illustrates the improved Coulombic efficiency of the lubricated TENG ($f_{M-Q} = 396$) compared to the non-lubricated device ($f_{M-Q} = 51$). This enhancement is attributed to the effect of liquid lubrication, which inhibits electrostatic breakdown. (e) Comparison of energy conversion efficiency between TENG with ($f_{M-Q} = 396$) and without ($f_{M-Q} = 51$) interface lubrication. All energy conversion efficiency of lubricated TENGs is higher than that of device without lubrication. (f) Long-term stability of TENG with ($f_{M-Q} = 396$) and without ($f_{M-Q} = 51$) lubrication. (g) Output energy density of represented works about TENGs.

mechanical-to-charge conversion, this study achieves a record output energy density of 11.9 J m⁻² cycle⁻¹, surpassing previous works (Fig. 5g).[11,13,36–40] Besides, the impacts of intrinsic material properties and lubrication performance on the f_{M-Q} of TENGs warrant further investigation, with the aim of establishing predictive correlations to optimize lubricant selection for TENG applications (Note S9).

Conclusions

In summary, our study highlights that energy consumption at elevated surface charge levels mainly drives by intense frictional heating and enhanced electrostatic forces. This significant energy dissipation underscores the longstanding trade-off between output performance and energy conversion efficiency in TENGs. To address this challenge, we introduce the mechanical-to-charge conversion factor (f_{M-Q}) as a quantitative metric to systematically guide the co-optimization of electrical output and energy utilization. Guided by this principle, we identified PA–PTFE tribo-pairs, which exhibit superior σ_{max} and f_{M-Q} compared to other tribo-pairs, as optimal candidates for TENG fabrication. Our theoretical analysis suggests that reducing the friction coefficient is an effective strategy to enhance f_{M-Q}. By implementing interface lubrication to mitigate energy dissipation from material wear, heat accumulation, and electrostatic breakdown, we increased f_{M-Q} from 51 to 396, achieving significant improvements in energy output, energy conversion efficiency, and stability. This led to a remarkable 17-fold improvement in energy conversion efficiency and a

10410 | *Energy Environ. Sci.*, 2025, **18**, 10403–10412

This journal is © The Royal Society of Chemistry 2025

record-breaking energy density of 11.9 J m^{-2} cycle^{-1}. This validates the potential for concurrent high output, efficiency, and stability, aligning with the demands of ambient micro/nano energy harvesting systems.

Additionally, the σ–F_f curve serves as a reliable indicator of the mechanical-to-charge conversion of TENGs, providing a guidance for selecting dielectric materials. The parameters related to k, which represent structural and dielectric material properties, may require further optimization to improve the output performance and energy conversion efficiency of TENGs (Note S10 and Fig. S20–S24).

Notably, this study reveals the dual effects of increased frictional contact area under high charge density conditions: on the one hand, it significantly enhances the surface charge density and thus improves the output performance of TENG, on the other hand, it concurrently exacerbates energy dissipation caused by electrostatic forces and frictional heating. Guided by the f_{M-Q} in proposed σ–F_f curve, these opposing effects are successfully decoupled, that suppresses energy dissipation (e.g., friction wear and thermal losses) while enhances charge density and output energy, which provides the direction for future optimization. Furthermore, interfacial lubrication not only inhibits interface breakdown to boost charge density under short-circuit conditions but also elevates Coulombic efficiency under applied external loads. Ultimately, the energy output density of TENG achieves a 3.4 times enhancement, whereas short-circuit charge density rises by only 30%, indicating that optimizing load-dependent efficiency metrics, rather than solely focusing on short-circuit charge density, is critical for maximizing TENG performance.

Experimental

Frication of the TENG

For the stator, a 40 mm × 20 mm × 5 mm acrylic block was cut using a laser cutter (PLS6.75, Universal Laser System). Two 20 mm × 20 mm × 0.05 mm electrodes were attached to the bottom surface of the acrylic block, maintaining a horizontal distance of 3.0 mm between them. PI was utilized as an insulator and was adhered to the edge of the electrodes. The triboelectric layer was constructed by adhering a foam layer to the acrylic substrate, followed by a 20 mm × 20 mm × 0.05 mm PI film. For the slider, a similar 20 mm × 20 mm × 5 mm acrylic block was cut using the same laser cutter. Subsequently, a foam layer was adhered to the acrylic substrate, followed by a 20 mm × 20 mm × 0.05 mm layer of either ETFE or polyamide PA film. Besides, squalene was specifically selected as the interfacial lubricant due to its unique triboelectric properties.

Characterization and electrical measurement

The sliding process was driven by a linear motor (TSMV120-1S). The short-circuit current and transferred charges of the TENGs were measured using a programmable electrometer (Keithley model 6514). The open-circuit voltage was determined with a potentiometer (Trek 347). The microscopy images of dielectric film surface were conducted using scanning electron microscopy (SEM, SU8020). The temperature on the PA surface was assessed using a handheld thermal imager (DS-2TPH10-3AUF). Three-dimensional optical surface profiler images were obtained with a three-dimensional topography profilometer (GT-X). The surface roughness of the dielectric film surface was examined using a surface roughness tester (TR200).

Author contributions

L. Zhou, D. Liu and J. Wang conceived the idea. L. Zhou and D. Liu designed the experiments and performed data measurements. Y. Gao, W. Qiao, D. Liu, Z. Zhao, L. Yin and X. Li helped with the experiments. L. Zhou drafted the manuscript. Z. L. Wang and J. Wang revised the manuscript and supervised this work. All the authors discussed the results and commented on the manuscript.

Conflicts of interest

There are no conflicts to declare.

Data availability

The data supporting this article have been included as part of the supplementary information (SI). Supplementary information is available. See DOI: **https://doi.org/10.1039/d5ee03995a**.

Acknowledgements

References

1 F. R. Fan, Z. Q. Tian and Z. L. Wang, *Nano Energy*, 2012, **1**, 328–334.

2 J. Chen, Y. Huang, N. Zhang, H. Y. Zou, R. Y. Liu, C. Y. Tao, X. Fan and Z. L. Wang, *Nat. Energy*, 2016, **1**, 16138.

3 H. Li, A. Berbille, X. Zhao, Z. Wang, W. Tang and Z. L. Wang, *Nat. Energy*, 2023, **8**, 1137–1144.

4 J. Wang, S. Li, F. Yi, Y. Zi, J. Lin, X. Wang, Y. Xu and Z. L. Wang, *Nat. Commun.*, 2016, **7**, 12744.

5 H. Zhao, M. Xu, M. Shu, J. An, W. Ding, X. Liu, S. Wang, C. Zhao, H. Yu, H. Wang, C. Wang, X. Fu, X. Pan, G. Xie and Z. L. Wang, *Nat. Commun.*, 2022, **13**, 3325.

6 L. Long, W. Liu, Z. Wang, W. He, G. Li, Q. Tang, H. Guo, X. Pu, Y. Liu and C. Hu, High performance floating self-excited sliding triboelectric nanogenerator for micro mechanical energy harvesting, *Nat. Commun.*, 2021, **12**, 4689.

7 Y. Zi, S. Niu, J. Wang, Z. Wen, W. Tang and Z. L. Wang, *Nat. Commun.*, 2015, **6**, 8376.

This journal is © The Royal Society of Chemistry 2025

Energy Environ. Sci., 2025, **18**, 10403–10412 | **10411**

8 D. Liu, L. Zhou, S. Cui, Y. Gao, S. Li, Z. Zhao, Z. Yi, H. Zou, Y. Fan, J. Wang and Z. L. Wang, *Nat. Commun.*, 2022, **13**, 6019.

9 H. Zou, Y. Zhang, L. Guo, P. Wang, X. He, G. Dai, H. Zheng, C. Chen, A. Wang, C. Xu and Z. L. Wang, *Nat. Commun.*, 2019, **10**, 1427.

10 Z. Liu, Y. Huang, Y. Shi, X. Tao, H. He, F. Chen, Z. Huang, Z. L. Wang, X. Chen and J. Qu, *Nat. Commun.*, 2022, **13**, 4083.

11 Y. Gao, L. He, D. Liu, J. Zhang, L. Zhou, Z. L. Wang and J. Wang, *Nat. Commun.*, 2024, **15**, 467.

12 Z. Zhao, Y. Dai, D. Liu, L. Zhou, S. Li, Z. L. Wang and J. Wang, *Nat. Commun.*, 2020, **11**, 6186.

13 W. He, W. Liu, J. Chen, Z. Wang, Y. Liu, X. Pu, H. Yang, Q. Tang, H. Yang, H. Guo and C. Hu, *Nat. Commun.*, 2020, **11**, 4277.

14 C. Shan, K. Li, Y. Cheng and C. Hu, *Nano-Micro Lett.*, 2023, **15**, 127.

15 K. Xiao, W. Wang, K. Wang, H. Zhang, S. Dong and J. Li, *Adv. Funct. Mater.*, 2024, **34**, 2404744.

16 H. Lee, J. Park, D. Jang, J. Shin, T. Im and J. Lee, *et al.*, *Nano Energy*, 2020, **75**, 104951.

17 H. Lee, H. Lee, H. Wang, S.-M. Kang, D. Lee, Y. Kim, J. Shin, Y.-W. Lim, K. Lee and B.-S. Bae, *Adv. Funct. Mater.*, 2020, **30**, 2005610.

18 J. Wang, C. Wu, Y. Dai, Z. Zhao, A. Wang, T. Zhang and Z. L. Wang, *Nat. Commun.*, 2017, **8**, 88.

19 J. Fu, G. Xu, C. Li, X. Xia, D. Guan, J. Li, Z. Huang and Y. Zi, Achieving ultrahigh output energy density of triboelectric nanogenerators in high-pressure gas environment, *Adv. Sci.*, 2020, **7**, 2001757.

20 S. Lin, L. Xu, C. Xu, X. Chen, A. Wang, B. Zhang, P. Lin, Y. Yang, H. Zhao and Z. L. Wang, *Adv. Mater.*, 2019, **31**, 1808197.

21 Y. Liu, W. Liu, Z. Wang, W. He, Q. Tang, Y. Xi, X. Wang, H. Guo and C. Hu, *Nat. Commun.*, 2020, **11**, 1599.

22 L. Cheng, Q. Xu, Y. Zheng, X. Jia and Y. Qin, *Nat. Commun.*, 2018, **9**, 3773.

23 W. Liu, Z. Wang, G. Wang, G. Liu, J. Chen, X. Pu, Y. Xi, X. Wang, H. Guo, C. Hu and Z. L. Wang, *Nat. Commun.*, 2019, **10**, 1426.

24 R. Budakian and S. Putterman, *Phys. Rev. Lett.*, 2000, **85**, 1000–1003.

25 H. Wistuba, *Wear*, 1997, **208**, 118–124.

26 T. Burgo, C. Silva, L. Balestrin and F. Galembeck, *Sci. Rep.*, 2013, **3**, 2384.

27 M. Wolloch, G. Levita, P. Restuccia and M. Righi, *Phys. Rev. Lett.*, 2018, **121**, 026804.

28 X. Li, P. Bista, A. Stetten, H. Bonart, M. Schür, S. Hardt, F. Bodziony, H. Marschall, A. Saal, X. Deng, R. Berger, S. Weber and H. Butt, *Nat. Phys.*, 2022, **18**, 713–719.

29 K. Sayfidinov, S. D. Cezan, B. Baytekin and H. T. Baytekin, *Sci. Adv.*, 2018, **4**, eaau3808.

30 Y. Xie, S. Wang, S. Niu, L. Lin, Q. Jing, J. Yang, Z. Wu and Z. L. Wang, *Adv. Mater.*, 2014, **26**(38), 6599–6607.

31 D. Liu, X. Yin, H. Guo, L. Zhou, X. Li, C. Zhang, J. Wang and Z. L. Wang, *Sci. Adv.*, 2019, **5**, eaav6437.

32 L. He, Y. Gao, D. Liu, Y. Hu, J. Shi, J. Zhang, X. Li, B. Jin, B. Zhang and Z. L. Wang, *Sci. Adv.*, 2024, **10**, eado5362.

33 J. Zhang, Y. Gao, D. Liu, J. Zhao and J. Wang, *Nat. Commun.*, 2023, **14**, 3218.

34 D. Liu, L. Zhou, Y. Gao, D. Liu, W. Qiao, J. Shi, X. Liu, Z. Zhao, Z. L. Wang and J. Wang, *Adv. Energy Mater.*, 2024, **14**, 2401958.

35 L. Zhou, D. Liu, Z. Zhao, S. Li, Y. Liu, L. Liu, Y. Gao, Z. L. Wang and J. Wang, *Adv. Energy Mater.*, 2020, **10**, 2002920.

36 J. Liu, L. Zhou, Y. Gao, P. Yang, D. Liu, W. Qiao, B. Zhang, Z. Zhao, Z. L. Wang and J. Wang, *Adv. Energy Mater.*, 2023, **13**, 2300410.

37 S. Fu, H. Wu, W. He, Q. Li, C. Shan, J. Wang, Y. Du, S. Du, Z. Huang and C. Hu, *Adv. Mater.*, 2023, **35**, 2302954.

38 L. Zhang, S. Liu, J. Wen, X. Huo, B. Cheng, Z. Wu, L. Wang, Y. Qin and Z. L. Wang, *Energy Environ. Sci.*, 2023, **16**, 3781–3791.

39 H. Wu, S. Wang, Z. Wang and Y. Zi, *Nat. Commun.*, 2021, **12**, 5470.

40 Y. Gao, J. Liu, L. Zhou, L. He, D. Liu, P. Yang, B. Jin, Z. L. Wang and J. Wang, *Energy Environ. Sci.*, 2024, **17**, 8734–8744.

10412 | *Energy Environ. Sci.*, 2025, **18**, 10403–10412

This journal is © The Royal Society of Chemistry 2025